HHS Public Access

Author manuscript

Biomaterials. Author manuscript; available in PMC 2023 May 01.

Published in final edited form as:

Biomaterials. 2022 May ; 284: 121483. doi:10.1016/j.biomaterials.2022.121483.

Synthetic hydrogels engineered to promote collecting lymphatic vessel sprouting

Joshua S.T. Hooks[1,2], **Fabrice C. Bernard**[1,3], **Ricardo Cruz-Acuña**[1,3], **Zhanna Nepiyushchikh**[1,2], **Yarelis Gonzalez-Vargas**[1,3], **Andrés J. García**[1,2,3], **J. Brandon Dixon**[1,2,3]

[1]Parker H. Petit Institute for Bioengineering and Bioscience, Georgia Institute of Technology 315 Ferst Dr. Atlanta, GA 30332

[2]George W. Woodruff School of Mechanical Engineering, Georgia Institute of Technology, 801 Ferst Dr. Atlanta, GA 30313

[3]Wallace H. Coulter Department of Biomedical Engineering, Georgia Institute of Technology, 313 Ferst Dr NW, Atlanta, GA 30332

Abstract

The lymphatic vasculature is an essential component of the body's circulation providing a network of vessels to return fluid and proteins from the tissue space to the blood, to facilitate immune call and antigen transport to lymph nodes, and to take up dietary lipid from the intestine. The development of biomaterial based strategies to facilitate the growth of lymphatics either for regenerative purposes or as model system to study lymphatic biology is still in its nascent stages. In particular, platforms that encourage the sprouting and formation of lymphatic networks from collecting vessels are particularly underdeveloped. Through implementation of a modular, poly(ethylene glycol) (PEG)-based hydrogel, we explored the independent contributions of matrix

---

Author contributions: J.B.D. and J.S.T.H. conceived the concepts. J.B.D., A.J.G., J.S.T.H., and R.C.A. designed the study. J.S.T.H., R.C.A., and F.C.B. performed the experiments and collected the data. J.S.T.H. conducted the data analysis. J.S.T.H., J.B.D., and A.J.G. wrote the manuscript.

Competing Interests: The authors have no competing interest to declare.

Declaration of interests

The authors declare that they have no known competing financial interests or personal relationships that could have appeared to influence the work reported in this paper.

Data and materials availability: Additional material and data which contributed to this study are present in the Supplementary Materials.

Code availability

Custom Matlab code used for image analysis of sprouting networks will be provided upon request.

CRediT author statement

Joshua Hooks: Conceptualization, Methodology, Investigation, Software, Formal Analysis, Writing – Original Draft, Visualization
Fabrice Bernard: Investigation, Formal Analysis, Writing – Review & Editing, Visualization
Ricardo Cruz-Acuña: : Investigation, Writing – Review & Editing
Zhanna Nepiyushchikh: Investigation, Formal Analysis, Writing – Review & Editing
Yarelis Gonzalez-Vargas: Methodology, Investigation, Visualization
Andrés García: Conceptualization, Methodology, Writing – Review & Editing, Supervision, Funding acquisition
Brandon Dixon: Conceptualization, Methodology, Writing – Review & Editing, Supervision, Project administration, Funding acquisition

elasticity, degradability, and adhesive peptide presentation on sprouting of implanted segments of rat lymphatic collecting vessels. An engineered hydrogel with 680 Pa elasticity, 2.0 mM RGD adhesive peptide, and full susceptibility to protease degradability produced the highest levels of sprouting relative to other physicochemical matrix properties. This engineered hydrogel was then utilized as a scaffold to facilitate the implantation of a donor vessel that functionally grafted into the host vasculature. This hydrogel provides a promising platform for facilitating lymphangiogenesis in vivo or as a means to understand the cellular mechanisms involved in the sprout process during collecting lymphatic vessel collateralization.

Summary:

A hydrogel was engineered to promote collecting lymphatic vessel sprouting. Systematic analysis of individual biomechanical and biochemical gel properties allowed local optimization of sprouting lymphangiogenesis in an in-vitro platform.

Introduction

The lymphatic vasculature in humans is critical for transporting over 8 liters of fluid per day, deemed lymph once entering the lymphatic system, from the interstitial tissue space back into the cardiovascular system(1). In addition to maintaining fluid homeostasis, lymphatics are primarily responsible for trafficking immune cells to lymph nodes, playing pivotal roles in inflammation and adaptive immune response(2, 3). Lymphangiogenesis is the process by which lymphatic endothelial cells (LECs) proliferate and form new vessels. It is the prevailing view that post-natal lymphangiogenesis is initiated from existing vasculature, including from lymphatic collecting vessels, which contain a luminal layer of LECs surrounded by specialized muscle cells referred to as lymphatic muscle cells (LMCs)(4–6). Whereas initial lymphatic capillaries are characterized by loosely connected lymphatic endothelial cells with specialized cell junctions, anchoring filaments to the interstitium, and no basement membrane, all of which served to facilitate fluid, protein, and cell entry to within the vessels, mature collecting vessels are structurally quite different from initial lymphatics. LMCs surrounding collecting vessels contain alpha-smooth muscle actin and other contractile filaments which are critical for the phasic contraction lymphatics undergo to generate lymph(4, 5). During prenatal development, research has begun to reveal facets of the complex signaling environment needed to recruit and orient LMCs along developing vasculature to form mature collecting vessels(7–9). However, it is unclear exactly how and if new lymphatic sprouts originating from collecting lymphatic vessels and formed during post-natal injury induced lymphangiogenesis, regain LMC coverage and restore their collecting vessel phenotype. Lymphangiogenesis has many parallels to angiogenesis, the formation of new blood vessels, and is promoted and inhibited by many of the same growth factors and signaling as the blood vasculature(6, 10). However, unique to LECs is a high surface expression of vascular growth factor receptor 3 (VEGFR-3), which binds with high affinity to vascular growth factors C and D (VEGF-C, VEGF-D)(7, 8, 11). In healthy individuals, lymphangiogenesis is induced during wound healing and inflammation, allowing for localized immune cell recruitment; however, lymphangiogenesis

is also associated with leaky and dysfunctional lymphatic vessels in certain pathological situations, including congenital disorders(12, 13).

In developed countries, lymphedema resulting from cancer treatments is the most common pathology of the lymphatic system. Lymphedema, or chronic swelling and fibrotic remodeling of the soft tissue due to lymphatic obstruction or dysfunction, significantly reduces patients' quality of life and remains incurable. Estimates of breast cancer related lymphedema (BCRL) vary from 15–30% of breast cancer patient survivors and is impacted by pre-existing lymph flow rates, the extent of lymph node dissections, and additional cancer treatments (14–17). As a treatment option, various methods of vascularized lymph node transfer and lymph node flap transfers have been shown to significantly reduce swelling in patients with lymphedema(18–21). The exact mechanism of this approach is not fully understood but appears to involve lymphangiogenesis of local and transplanted lymphatic vasculature to nearby lymph nodes or venous outlets(22, 23). If induction of neo-lymphangiogenesis is the primary mechanism, a transplanted lymph node may not be needed if an alternative treatment can induce and guide organized lymphangiogenesis across the wound. For example, VEGF-C gene therapy alone was shown to regenerate collecting lymphatic vessels after surgical resection of axillary lymph nodes allowing for lymph transport across the resected area (24).

To develop a biomaterial platform capable of augmenting sprouting lymphangiogenesis from a collecting lymphatic vessel, we engineered a 3D hydrogel system through optimization of various parameters to support vessel sprouting from cultured, rat-derived lymphatic collecting vessel segments. Hydrogels were formulated using a four-armed poly(ethylene glycol) (PEG) macromer with maleimide groups at each terminus (PEG-4MAL) that were conjugated to cell adhesive ligands and crosslinking peptides. The modular nature of the synthetic hydrogel allows for greater understanding of the biophysical and biochemical properties of the extracellular matrix (ECM) that guide lymphangiogenic sprouting in a controlled and systematic fashion. Early 3D lymphangiogenesis models involve culture of lymphatic tissue in "natural" matrices such as collagen gels(25, 26), where all gel properties are intricately tied to collagen concentration(27, 28). Independently tuning the PEG weight percentage, crosslinking or adhesive peptide type and density alters the biophysical and biochemical signals(29–31) leading to significant changes in tissue phenotype(29, 32–34), a phenomenon also recently demonstrated in the formation of lymphatic cord-like structures by lymphatic endothelial cells cultured in hyaluronic acid hydrogels of varying stiffness(35). There has been an emergence of studies over the past few years demonstrating the feasibility of synthetic matrices or hydrogels to support in vitro 3D lymphangiogenesis of lymphatic endothelial cell capillary networks composed of lymphatic endothelial cells, often through the inclusion of support cells(36–41) or lymphatic endothelial progenitor cells(42). However, it remains unclear the extent that these platforms can be engineered to support sprout formation and coordinated LEC and LMC from a collecting lymphatic vessel, thus we sought to take advantage of the PEG-4MAL hydrogel system to engineer such a tissue and determine the effects of stiffness, degradability, and adhesive peptide type and density on vessel network formation. Once an optimal lymphangiogenic gel formulation was identified, we demonstrate the utility of this synthetic lymphangiogenic hydrogel to support

the incorporation and collateralization of local and transplanted lymphatic collecting vessels following injury.

Methods

PEG-4MAL hydrogel synthesis

To prepare PEG hydrogels, PEG-4MAL macromer (MW 22,000; Laysan Bio) was dissolved in 4-(2-hydroxyethyl)piperazine-1-ethanesulfonic acid (HEPES) buffer (20 mM HEPES in DPBS, pH 7.4) at 2.5x the final density. Adhesive and cross-linking peptides were custom synthesized by AAPPTec. Adhesive peptides that were used include RGD (GRGDSPC), GFOGER (GYGGGP(GPP)$_5$GFOGER (GPP)$_5$GPC), RDG (GRDGSPC), and GAOGER (GYGGGP(GPP)$_5$GAOGER (GPP)$_5$GPC), where O = hydroxyproline. Adhesive peptides were dissolved in HEPES at 10.0 mM (5X final ligand density) and mixed with PEG-4MAL at a 2:1 PEG-4MAL/ligand ratio to generate a functionalized PEG-4MAL precursor. After at least 15 min, the functionalized PEG-4MAL precursor solution was further diluted using HEPES buffer at a 3:1 functionalized PEG-4MAL/HEPES ratio. Bis-cysteine cross-linking peptide GPQ-W (GCRDGPQG↓IWGQDRCG; ↓ denotes enzymatic cleavage site) was dissolved in HEPES at 5X the density that corresponds to 1:1 maleimide/cysteine ratio after accounting for maleimide groups reacted with adhesive peptide. Non-degradable (or 0% degradable) gels were made by exchanging GPQ-W with the non-enzymatically degradable crosslinking agent, PEG-DT (hexa(ethylene glycol) dithiol).

Hydrogel characterization

The storage moduli of hydrogels of different PEG weight percentages were assessed by dynamic oscillatory strain and frequency sweeps performed on an MCR 302 stress-controlled rheometer (Anton Paar) with a 9-mm diameter, 2° cone, and plate geometry (Supplementary Figure 1). Oscillatory frequency sweeps were used to examine the storage and loss moduli (ω = 1–100 rad s-1) at a strain of 2.3%.

Collagen gel synthesis

Collagen gels were prepared using a stock solution (5 mg/mL, Gibco - A1048301) of rat tail collagen, type 1, concentrated at five times the final desired concentration. Approximately 3.75 volumes of type 1 collagen, 3.75 volumes of sterile H2O, 1 volume of HEPES (200mM), 1 volume of 10X DMEM, 0.5 volumes of NAHCO3 (74mg/mL) were mixed together on ice and kept cold. Immediately before encapsulation of tissue, pH was brought to 7.4 using NaOH and 20 μL of this collagen solution was added to each well.

Lymphatic isolation and encapsulation

Isolation of Rat Lung Draining Lymphatic Vessels (LLV)—Lymphatic collecting vessels from the mediastinal region that drain downstream of the lungs, running alongside the left phrenic nerve, were isolated from surrounding connective tissue in the chest cavity of adult male Sprague Dawley rats (350–400 g, 10–12 weeks). In brief, rats were euthanized and immediately shaved along the chest. The chest cavity was opened and the lung and heart were gently pulled to the side, exposing the phrenic nerve located above the lungs. About 5–6 mm of lymphatic collecting vessel that travels parallel to the nerve was mechanically

separated from the surrounding fat tissue, taking care to keep the vessel from drying out by frequent application of Dulbecco's Phosphate-Buffered Saline (DPBS). This section of lymphatic vessels was termed the lung draining lymphatic vessel (LLV). After being cleaned from surrounding tissue, the vessel segment was removed and transported to a petri dish of DPBS for further cleaning and to be cut into roughly 300-micron long segments. To form hydrogels, an individual vessel segment was carefully placed into a solution of the cross-linking peptide in a 24 well plate. A solution of the adhesive peptide-functionalized PEG-4MAL macromer was then mixed in and allowed to polymerize for 15 min before the addition of growth medium. All animal procedures were performed in compliance with procedures approved by the Georgia Institute of Technology Internal Animal Care and Use Committee (IACUC).

Tissue culture

Culture Protocol for LLV During Characterization of Response to PEG Hydrogel Properties—Segments were cultured in an endothelial basal medium (EBM) formulation as previously described(43). This consisted of EBM (Lonza,) supplemented with 20% FBS (Atlanta Biologicals), 1% penicillin-streptomycin-amphotericin B (Gibco), 1% Glutamax (Gibco), 0.1% DBcAMP (Sigma), and 0.1% hydrocortisone acetate (Sigma). Vessel segments were cultured for a total of 7 days and media was changed on days 3 and 5.

In-vitro drug assay

Rat LLV samples were cultured in the standard EBM formulation until day 5. Samples were then treated with docetaxel (1μM in ethanol) or carboplatin (1μM in PBS) or in a vehicle control of ethanol.

For rapamycin, at day 5, 20 nM or 100 nM rapamycin was suspended in EBM and applied to the samples and reapplied at day 8 before analysis and/or fixation at day 10. An equal volume of DMSO was added to untreated samples as a vehicle control. Samples that had not begun sprouting by day 5 were discarded.

Live/dead assay

Calcein-AM and Toto-3 (Thermo Fisher) were used as a live and dead stain, respectively, to determine the viability of the tissue within the hydrogel at day 7. Each stain was mixed with cell culture media at a 1:1000 ratio and incubated with the tissue samples at 37°C for 1 hour. Samples were rinsed with PBS before imaging via confocal microscopy followed by fixation in 4% paraformaldehyde (PFA) for 10 minutes. Images were collected on an inverted confocal microscope (Zeiss LSM 700B). Images of larger sizes are stitched images of z-stacks at different x-y locations, altering the size of the image but maintaining the same resolution for analysis.

Sprouting analysis

Sprouting from vessel segments were analysed following the live/dead stain using image analysis code developed in MATLAB (Appendix A). Samples were imaged with an inverted confocal microscope (Zeiss LSM 700B) using a 5X objective (0.16 numerical aperture and working distance of 12.10 mm). This code binarized the max intensity projections of the live

stain determined the sprout length and branching complexity. If samples did not test positive for the live stain they were not included in the sprouting analysis. The code requires the user to manually select the location of the implanted vessel segment and then sets concentric squares around the selected point to determine the quantity of tissue along the perimeter. By assessing the percent of tissue vs blank space along the perimeter the max length of sprouts and number of individual sprouts could be assessed. All conditions used in the sprouting analysis have 6 or more biological replicates pooled from at least 2 independent experimental runs.

Immunostaining and imaging

Lymphatic samples from rat cultured within the PEG hydrogels were stained to assess morphology and cell type. General morphology was assessed with a phalloidin based F-actin stain (Invitrogen). Cell lineage was determined via staining for expression of alpha-smooth muscle actin (αSMA, Mouse IgG2a, Sigma - A2547) and vascular endothelial growth factor receptor-3 (VEGFR-3, Rabbit IgG, Invitrogen - PA516871). Fixed tissue samples within the gels were permeabilized with 0.5% Triton-X for 20 minutes and then rinsed 3 times. After the third rinse, samples were blocked for 1 hour in a blocking solution composed of phosphate buffered saline (PBS) with 10% goat serum (the secondary antibody host) and 2% bovine serum albumin (BSA). The blocking solution was then removed, and samples were incubated with primary antibodies suspended in 2% BSA (1:200) overnight at 4°C on a rocker. The samples were then rinsed three times and then rocked in a solution of secondary antibodies (1:400) for two hours at room temperature. After a final three rinses the samples were then imaged using an inverted confocal microscope (Zeiss LSM 700B). For Figure 6 A&B, a 10X objective (0.3 numerical aperture and working distance of 5.2mm) was used for the base images. A 40X objective (1.4 numerical aperture and working distance of 0.130 mm) was used for the magnified regions in Figure 6 C&D. Images in Figure 6 were taken with the 20X objective (0.8 numerical aperture and working distance of 0.550 mm). Base images in Figure 7 A,B were taken with a 5X objective (0.16 numerical aperture and working distance of 12.10 mm) and the magnified region (Figure 7 C) was taken with the 20X objective.

Nonspecific isotype controls of mouse IgG2a (Sigma - M5409), rabbit IgG (Sigma - I5006), and mouse IgG1 (Sigma - 5284) were used at the same concentration as the primary antibodies on samples to ensure that there was no non-specific binding of the antibodies (Supplementary Figure 2). The same staining and imaging protocols were implemented as the primary antibodies described previously.

Additionally, these antibodies were used to stain an intact lung draining lymphatic vessel to ensure positive staining of the lymphatic muscle cells (αSMA^{+}) and lymphatic endothelial cells (VEGFR-3^{+}) shown in Supplementary Figure 3. After careful dissection, the intact lymphatic vessels were fixed in 2% paraformaldehyde in PBS for 60 min and washed in PBS 3 times for 5 minutes each. The vessel was permeabilized in 0.1% PBST (PBS with 0.1% Triton X-100) for 20 minutes and incubated in a blocking solution (1% BSA, 5% normal serum in PBS) for 1 hr at room temperature. The vessel was then cut into 2 segments. One segment was incubated at 4°C overnight with the primary antibodies in blocking solution.

The second section was given the same treatments except the primary antibody was replaced with the corresponding isotype control. Both segments were washed three times in PBS, both intraluminal and abluminal, before incubation with the secondary antibodies for 1 hr at RT. The vessel segments were washed in PBS 3 times for 5 minutes. The vessels were then cannulated and tied onto 2 glass pipettes, pressurized at 2 cm H_2O, and secured to the stage of a multiphoton confocal microscope (Zeiss 710 NLO) for imaging. The vessels were scanned with a Zeiss PL APO 20X (0.8 NA) objective.

ImageJ Image Analysis

The ImageJ plugin angiogenesis analyzer (Carpentier et al., 2012) was used to construct binary tree skeletons of sprouting networks to quantify sprout length and nodes/mm of the lymphatic networks in the PEG-4MAL and collagen gel cultures. Additionally, the ImageJ plugin coloc 2 was used to quantify stain colocalization of smooth muscle actin-alpha and vegfr-3. IN brief, this software performs pixel intensity correlation over space and produces a 2D histogram with regression line and calculates the Pearerson's r coefficient.

GFP Tissue Transplantation with PEG Hydrogels

Ubiquitously green fluorescent protein (GFP) expressing Sprague Dawley rats (RRRC:0065 [SD-Tg(UBC-EGFP)2BalRrrc]) were purchased from the Rat Resource & Research Center. Animals were anesthetized via injections of ketamine (40mg/kg) and dexdomitor (0.13mg/kg) and the left hindlimb was shaved of hair. A near infrared (NIR) dye (IRDye® 800CW), conjugated to 20kDa PEG polymers, were injected into the footpad. Due to the size of the polymer this NIR tracer is drained from the footpad interstitium exclusively by the lymphatic system. Imaging through the skin revealed two lymphatic collecting vessels that drain lymph formed in the foot pad to the popliteal lymph node and travel parallel to the saphenous vein. A 1–2cm long segment of the two parallel collecting vessels was resected proximal to the ankle (Figure 7A). These vessels were segmented into 3–5mm long segments and stored in sterile saline solution. In non-fluorescent Sprague Dawley rats, the same segments of collecting vessel were isolated and discarded. One segment of the GFP expressing collecting vessel was placed along the lateral side of the saphenous vein where the host's collecting vessel was removed. Ten microliters of 10%PEG – 2mM RGD gel was carefully polymerized over the vessel segment and the skin sutured close over the gel and wound. Gels were fabricated as outlined in section 3.2.1. The animals were risen with antisedan (1.3mg/kg) and carefully monitored following recovery. Lymphatic repair in the wound site was assessed using NIR imaging on days 7, 14, and 28 following surgery. This procedure was carried out on 2 adult male rats. All animal procedures were performed in compliance with procedures approved by the Georgia Institute of Technology Internal Animal Care and Use Committee (IACUC).

On day 28, the animal was administered an intradermal injection, 20 microliters, of fluorescent lectin (Vector Laboratories - DL-1178–1, DyLight® 649, 1mg/mL), that was passively drained by the lymphatics due to size exclusion from the blood vasculature. After 10 minutes, animals were then euthanized and the entire wound site, including the saphenous vein, was isolated and immediately frozen in optimal cutting temperature (OCT) compound. Tissue slices were stained with a nuclear DAPI stain, for GFP expressing

cells, and VEGFR-3 expressing cells. Samples were fixed using a 4% paraformaldehyde (PFA) suspended in a physiological saline solution for 10 minutes then rinsed three times with phosphate buffered saline (PBS). Sections were permeabilized with a 0.5% Triton-X solution at room temperature for 10 minutes and rinsed again three times in PBS. Blocking of samples was done in a PBS solution containing 2% bovine serum albumin, BSA and 10% goat serum for 1 hour at room temperature. Following this, primary antibodies for GFP and VEGFR-3, suspended in the 2% BSA solution (1:100), were applied to the samples for one hour on a plate rocker. The samples were rinsed in PBS (3x) before application of a fluorescent secondary antibody solution in 2% BSA (1:200) for 1 hour at room temperature on a shaker. Samples were rinsed two times in PBS before imaging. Additional sections were also stained with isotype control antibodies for the GFP antibody (chicken IgY) and VEGFR-3 (polyclonal rabbit IgG). The maximum intensity from these controls were subtracted from the actual stains to eliminate background and non-specific fluorescence.

Statistics

GraphPad Prism version 7.01 was used for statistical analysis. Kruskal-Wallis test followed by Dunn's multiple comparisons test were used for comparisons between multiple experimental groups at the end of each culture period. The biological replicates for the 10% PEG – 2mM RGD gel, tested for multiple experimental conditions, are grouped and presented in Figures 2–5. All analyses were considered statistically significant at $p<0.05$. Error bars on all data points are standard deviation. Grubbs test for statistical outliers was used to remove one outlier from the 1.00 mg/mL collagen gel condition. An F test was used to determine the significance of a non-zero slope for the RGD concentration vs sprouting curves in Figure 4)

Results

PEG hydrogel properties modulate lymphatic sprouting

PEG-based hydrogels were formulated as an alternative to naturally derived ECMs (e.g. collagen gels), which are limited by the inability to uncouple mechanical and biochemical properties. The four-armed PEG macromer was terminated with maleimide groups (PEG −4MAL) which allow for functionalization with peptides and modulation of hydrogel properties as shown in Figure 1.

We sought to tune the biomechanical and biochemical properties of a PEG-4MAL hydrogel in order to optimize their lymphangiogenic capacity. Segments of lung-draining lymphatic collecting vessels (LLV) dissected from rat tissue were embedded in PEG-4MAL hydrogels of different formulations. The weight percentage of PEG polymer, type of adhesive peptide, and crosslinker sensitivity to proteases were altered independently to examine the impact of each parameter on sprout formation. Using computerized image analysis, the resulting lymphatic network emerging from the embedded segment was quantified after 7 days of culture. This image processing technique used a concentric square grid centered at the implanted tissue segment to determine the maximum sprout length and the average number of intersections sprouts made with each concentric square boundary. The average number of intersections metric reflects the number of sprouts formed from the initial tissue segment.

Unless otherwise stated, hydrogels were 10% PEG, functionalized with RGD (2.0 mM), and crosslinked with the protease-degradable crosslinker GPQ-W (GCRDGPQGIWGQDRCG).

Rat LLV sprouting was sensitive to the polymer density of the PEG hydrogel, which directly controls the mechanical properties of the PEG-4MAL gel (Supplementary Figure 1)(30). The length of sprouts within the PEG-4MAL hydrogel and the number of sprouts branching from the embedded segment were maximal at an intermediate polymer density (10%) compared to 6%, 8%, and 12% PEG polymer densities (Figure 2).

RGD is a conserved adhesive peptide present in fibronectin and other ECM proteins and binds with high affinity to a variety of integrins(44–46). LLV segments in PEG-4MAL hydrogels functionalized with RGD peptides exhibited significantly higher sprouting when compared to its inactive scrambled peptide RDG (GRDGSPC) that does not support cell adhesion (Figure 3). PEG hydrogels presenting the collagen I-derived GFOGER (GYGGGP$(GPP)_5$GFOGER $(GPP)_5$GPC) triple helical peptide did not support the same length or number of sprouts and produced sprouting that was not different from its scrambled peptide GAOGER (GYGGGP$(GPP)_5$GAOGER $(GPP)_5$GPC) or RDG. Notably, PEG gels with the scrambled peptides supported low levels of sprouting at day 7 of culture.

The density of RGD adhesive peptide in synthetic hydrogels has been shown to regulate functions such as endothelial cell proliferation, ECM deposition, and gene expression, altering expression of a variety of genes in different cell types(47–50). We next examined the effects of RGD density on lymphatic sprouting. A constant 2.0 mM total density of adhesive peptide was maintained by altering the ratio of RGD peptide and scrambled inactive RDG peptide (0–2.0 mM). The upper limit of 2.0 mM concentration was motivated by similar studies using similar PEG gel systems(51) which show that oversaturation of RGD peptides will impair sprouting. Both average sprout length and the average number of intersections increased linearly with RGD density (Figure 4). These results demonstrate that the polymer density (mechanical properties) and RGD peptide density control lymphatic sprouting.

Finally, the impact of gel degradability on sprouting phenotype was examined. Because of the nanoscale mesh size of thesthe optimise gels(29, 52), degradation is critical for cell migration and sprout formation within the hydrogel network. By altering the ratio of the protease-degradable, GPQ-W, crosslinker, to a non-degradable, PEG-DT (hexa(ethylene glycol) dithiol), crosslinker, we altered the susceptibility of the hydrogel to protease degradation. Protease degradable gels (“100%” degradable) were crosslinked entirely with GPQ-W while non-degradable gels (“0%” degradable) were crosslinked with PEG-DT. A third hydrogel condition was crosslinked with a 1:1 ratio of GPQ-W and PEG-DT (“50%” degradable). Hydrogels crosslinked with GPQ-W peptides supported significantly longer and a higher number of sprouts than other conditions (Figure 5).

Synthetic hydrogels and collagen gels elicit distinct lymphatic sprouting morphologies

A PEG-4MAL hydrogel containing 10% PEG, presenting 2.0 mM RGD, and 100% degradable crosslinks optimized lymphatic sprouting from implanted lymphatic vessel segments. We sought to compare lymphatic network formation in the optimized PEG-4MAL

hydrogel to type I collagen hydrogels. Relative to collagen gels, sprouts in PEG hydrogels were more structured, with multiple cells aligning into well-defined, continuous sprout extensions by day 7 (Figure 1 A). Unlike PEG hydrogels, cells composing the lymphatic vessel appeared to proliferate radially from the implanted vessel segment in collagen gels and did not organize into multi-cellular organized sprouts (Figure 1 G). Increasing magnification (Figure 6 C & D) clearly show the morphological differences between the sprouts in the PEG gels compared to cell proliferation in the collagen gels at day 7 of culture. The organization of the cell network was measured using ImageJ's angiogenesis analyzer plug in which overlays the lymphatic networks with discreet segments joined at nodes (Figure 6 E & F). This analysis allowed for quantification of the unique morphological differences between PEG and collagen gels; demonstrating that the lymphatic network in the PEG-4MAL hydrogel had, on average, longer segment lengths between nodes, with fewer total number of segments and nodes (Figure 6 G). This distinct outward proliferative morphology of the lymphatic cell network was evident in collagen gels at multiple concentrations (Supplementary Figure 4).

LEC and LMC cooperatively migrate to form sprouts within PEG hydrogels

Sprouting lymphatic segments embedded in the optimal PEG gel formulation were stained for lymphatic cell markers to assess cell type, phenotype, and organization. Alpha-smooth muscle actin (αSMA) staining identifies LMCs and/or myofibroblasts, whereas vascular endothelial growth factor 3 (VEGFR-3) identify LECs (Figure 7). In 10% PEG gels presenting 2.0 mM RGD and 100% degradable crosslinks, LECs within the sprouts stained positive for VEGFR-3 (Figure 7A). Furthermore, sprouts within the synthetic PEG-4MAL hydrogel contained αSMA positive cells aligned with VEGFR-3 positive cells. *In vivo*, this co-localization of multiple cell types along a sprout is indicative of a mature collecting lymphatic vessel. In contrast, cells within the collagen gel generally stained positive for either VEGFR-3 or αSMA, but with no apparent co-localization or organization (Figure 7 B). 2D intensity histograms quantify staining correlation of the VEGFR-3 and SMA stains in the PEG-4MAL condition compared to collagen gels (Figure 7 D) with Pearson's r values of 0.72 and 0.44 respectively. The high staining colocalization in PEG-4MAL compared to collagen gel conditions can be seen visually in the magnified regions of interest of each merged image (Figure 7 D).

Lymphangiogenic PEG hydrogel to deliver lymphatic tissue following surgical resection

Lymph transport can be visualized and measured over time via injection of NIR labelled PEG tracer injected into the footpad. Due to size exclusion of blood vasculature, the PEG tracer is selectively up taken by the lymphatic vasculature and real-time transport can be imaged through the skin. This reveals two primary lymphatic collecting vessels that drain the footpad interstitial fluid. A lymphatic injury model was implemented, removing both of these lymphatic collecting vessels which run along the saphenous vein distal to the popliteal lymph node. A segment of GFP expressing collecting vessel harvested from a GFP rat (Rat Resource & Research Center) was implanted into the wound site of a non-fluorescent host after the two lymphatic collecting vessels that drain the foot pad were resected (Figure 6 A-C). After one week, lymph flow along the limb, as tracked with NIR labelled PEG tracer injected into the footpad, seemed to have been established through a network of smaller

collateral vessels (Figure 6D). By day 28, flow through a single mature collecting vessel was restored across the wound site (Figure 6E). On day 28, following the injection and imaging of the NIR labelled PEG tracer, 20uL of fluorescent lectin was injected into the interstitium of the foot pad on day 28 and drained by the lymphatics into the popliteal lymphatics due to size exclusion from the blood capillaries (Figure 6F). Imaging the fluorescent lectin (emission wavelength: 690nm) through the skin matched perfectly with NIR fluorescence (emission wavelength: 889nm) confirming lymphatic specific drainage of the lectin. The skin above the wound site was carefully removed and underlying tissue was resected along the dotted lines. After section and staining, the lymphatic collecting vessel draining the foot was identifiable via the residual lectin stain (Figure 6G & H) demonstrating functional uptake into the vessel from the injection site at the footpad. Additional stainig of these slides show widespread GFP expression of local vasculature and weak VEGFR-3 expression (Figure 6 I-K).

Discussion

Utilizing synthetic PEG-4MAL hydrogels, we have demonstrated that lymphatic sprouting from collecting vessels is regulated by matrix stiffness, RGD density, and susceptibility to protease degradability. Lymphatic tissue cultured within these gels reproducibly organizes into lymphatic networks with sprouts staining for VEGFR-3$^+$ LECs and αSMA$^+$ cells, similar to mature vessels *in vivo*. This work demonstrates the applicability of PEG-4MAL hydrogels, engineered to optimize lymphatic sprouting, to study lymphatic function, responsiveness to intervention, and potential for in-vivo application. Finally, we demonstrate the capacity for host's lymphatic collecting vessels to connect with transplanted lymphatic tissue delivered with the lymphangiogenic PEG hydrogel formulation.

The consistency and tunability of PEG-4MAL hydrogels revealed several understudied regulators of lymphatic sprouting and a unique sprouting phenotype. The RGD adhesive peptide allowed for the most robust sprouting phenotype compared to type I collagen peptides. This is in alignment with studies that show formation of initial lymphatic capillary networks from LECs encapsulated in 3D fibrin gels, which present RGD domains(38, 53). Both the αvβ3 and α5β1 integrin dimers, which bind with high affinity to the RGD peptide, are documented to play a role in either lymphangiogenesis(54) or angiogenesis(55). Deposition of adhesive matrix proteins produced by cells of the implanted tissue likely allowed for eventual but delayed sprouting lymphangiogenesis in the RDG and GAOGER presenting hydrogels. Incorporating GFOGER, or other adhesive peptides, in combination with RGD could reveal novel or synergistic effects in future studies. Varying the weight percentage of PEG revealed a relative maximum in sprout length and number. 10% PEG hydrogels have a higher storage modulus (680 Pa) compared to a 2 mg/mL collagen gel (20 Pa(51)), and this finding may indicate a stiffness-based cue which promotes lymphangiogenesis during injury based interstitial remodelling. This finding may have important implications for remodelling in lymphedema, where tissue fibrosis is routinely observed in the affected limb and may adversely influence the formation of new collaterals from the intact collecting vasculature. Finally, as previously stated, cells within the sprouts of these lymphatic networks stained positive for αSMA which indicates partial LMC coverage. This has not been documented in similar studies using segments of mouse thoracic

duct in collagen gels(25), as sprouts in these tissues lacked αSMA$^+$ cell coverage. Cyclic LMC contraction, critical for lymphatic fluid transport, is dependent on pressure and stretch-sensitive calcium channels(56, 57), so it is unknown if these αSMA+ cells have the capacity to support intrinsic pumping.

As previously stated, the lymphangiogenesis observed in collagen gels in this study was morphologically distinct from the sprouting observed in the PEG hydrogels. This difference in sprouting morphology was clear at early time points, with lymphatic sprouting/proliferation in collagen gels losing any clear organization by day 5 (Supplementary Figure 5). Additionally, this was distinct from similar studies in which mouse thoracic duct segments were cultured in collagen gels(25). Therefore, we explored the impact of species, lymphatic anatomical location, and media conditions on resulting lymphatic networks (Supplementary Figure 6). When these factored were more closely matched to previous studies, the lymphatic sprouting morphology observed in those studies were repeated. This demonstrates the heterogeneity of lymphatic vessel culture and encourages further research to optimize lymphatic culture conditions based on region and species. Regional heterogeneity of lymphatic vessel function has been well documented(3, 58–60), but this synthetic gel provides a platform to determine how regionally distinct cellular phenotypes impact sprouting capacity and sensitivity to matrix cues, which is currently unknown. This platform is further advantageous in its capacity to be functionalized with matrix binding motifs from a variety of ECM matrix components, recreating regional heterogeneity. Lymphatic endothelial cells have been cultured in a variety of 3D matrix systems with extensive proliferation observed in predominantly fibrin gels (38, 61, 62). These results align well with the enhanced sprouting we find in the PEG-4MAL gel functionalized with RGD compared to GFOGER (a collagen mimetic peptide). Another matrix component of interest is hyaluronic acid (HA), which has been shown to interact with the HA receptor, LYVE-1, on LECs and induces LEC migration and lymphangiogenesis as it degrades (63, 64). While not tested here, HA or other matrix ligands can be incorporated into the PEG hydrogel to better understand how they regulate lymphatic function and regeneration. The distinct advantage of the PEG-4MAL platform for future studies is the control it gives the user to present specific matrix properties independently or in controlled ratios to precisely and repeatably probe these questions. The optimized 10% PEG- 2mM RGD hydrogel is a stable platform capable of supporting continued lymphatic sprouting through at least 20 days of culture with no visible signs of degradation (Supplementary Figure 7). Additionally, like naturally derived matrices, the PEG-4MAL gel is easily degradable which allow for further phenotyping of the resulting sprouting networks via flow cytometry or quantitative PCR.

While our knowledge of the molecular signaling regulating lymphangiogenesis of initial lymphatic capillaries has grown substantially, in large part due to studies that are afforded through in vitro models, our understanding of the mechanisms driving sprout formation from mature collecting vessels, and the participation of LMCs and their recruitment to these newly formed sprouts is severely limited. This platform, which supports coordinated LMC and LEC recruitment during the sprouting process, has potential to provide insight into the molecular signals responsible for this process such as growth factors, cytokines, and clinical drugs. For example, implementing a 10-day culture period, we conducted a preliminary study to explore the role of chemotherapeutics, docetaxel and carboplatin, on sprout

formation (Supplementary figure 8). In brief we found that docetaxel, but not carboplatin inhibited sprout formation. Docetaxel has previously been noted to inducing swelling in patients(65, 66) but the impact on multicellular lymphatic tissue has not been explored in-vitro. Previous in-vivo studies showed enhanced lymphangiogenesis upon treatment with docetaxel(67) but our results would indicate that this may occur through secondary pathways involving the tumor and other cellular regulators of lymphatic function.

In addition to serving as a platform for mechanistic *in vitro* studies, these lymphangiogenic PEG-4MAL hydrogels could serve as a scaffold to support in lymphatic regeneration *in vivo*. PEG hydrogels of similar formulations are beneficial in several animal models for organoid transplant or improved wound healing(31, 68, 69). Autologous lymph node transfers and lymph node flap transfers are promising emerging therapies for patients suffering from lymphedema(18, 19, 21, 70), yet these procedures assume that the implantation of the node itself will provide the necessary biochemical cues to support recruitment of mature collecting vessels to incorporate the node into the host's lymphatic vasculature as no such connections are physically made during the surgery. Research over the last decade have demonstrated that growth of functional lymphatic vasculature across a wound or to an implanted lymph node can be enhanced with scaffolding and growth factors(71–73). More recently, many of these studies have led to clinical trials using Lymfactin®, an adenoviral VEGF-C therapy(73), and BioBridge, an aligned nanofibrillar collagen scaffold (72), to enhance the efficacy of transplanted lymph nodes to treat and prevent lymphedema. This study demonstrates that our engineered PEG hydrogel incorporated with lymphatic tissue allows for functional lymph flow across small resections in the draining lymphatic network. The transplanted GFP expressing lymphatic vessel was functionally integrated into the host's lymphatic vasculature as indicated by intraluminal lectin staining of the GFP positive lymphatic vessel. The lumen of the lectin coated lymphatic vessel was over 50 microns wide and was 1–2inches downstream from the injection site, indicating that it is a mature lymphatic collecting vessel but additional staining for LMC coverage would be needed to confirm. The use of these lymphangiogenic PEG hydrogels as a scaffold could enhance functional lymphatic regeneration and connect collecting lymphatic vessels to transplanted lymph nodes or be a preventative measure following lymph node resection. In addition, they serve as a unique experimental platform for investigating the molecular mechanisms and the role of the microenvironment in sprouting lymphangiogenesis originating from collecting lymphatic vessels.

Supplementary Material

Refer to Web version on PubMed Central for supplementary material.

Acknowledgments

Funding:

This work was supported by the National Institutes of Health [NIH R01 HL113061, R01 HL133216, R01 AR062920, R01 AR062368].

Data availability

All source data generated or analysed during this study are available in this article, the supplementary files, and in publicly available repositories. All images and measured values can be found in the public repository, figshare (10.6084/m9.figshare.12818351 and 10.6084/m9.figshare.12818339, respectively).

Appendix A: Matlab Code to quantify sprouting length and average branch number:

```
close all
clear
clc


%User must update folder location and make sure all images are numbered
PicLoc ='C:\Users\X\OneDrive\Documents\Hydrogel\5x Live\num\'; %Example
PicName='1'; %Images must be numbered starting with 1
PicType= '.tif';

NumIm=3; %User input for specific # of images in the folder
for v=1:NumIm
PicName=num2str(v);
I = imread(strcat(PicLoc,PicName,PicType));
% I=imadjust(I);
% imshow(I)
figure
imagesc(I)



[x,y]=ginput(1); %User selects center of vessel (gives decimals)
xO(v)=round(x,0);
yO(v)=round(y,0);
end
close all
%-----------------------------------


for v=1:NumIm
PicName=num2str(v);
I = imread(strcat(PicLoc,PicName,PicType));

pix2mm=491.5;
```

```
inc=7;
aO = inc; %tracing for background sample and vessel core sizes
a = inc; %First tracing (52pixels is about 0.25mm)

[Isizex,Isizey]=size(I);
Squarelimit=min(Isizex,Isizey);

maxdist=round((Squarelimit/2)/inc);
th=9; %thickness of square to average pixel values across

I4 = imread(strcat(PicLoc,PicName,PicType));
I5=imadjust(I4);
% figure
% imshow(I5)
level = graythresh(I5);
level=(level-0.25*level); %Usuallt 0.15
bw = im2bw(I5,level);
% bw = im2bw(I5);
bw = bwareaopen(bw,10);
% figure
% imshow(bw)


filled = imfill(bw, 'holes');
% filled = imfill(bw);

% figure
% imshow(filled)

holes = filled & ~bw;
bigholes = bwareaopen(holes, 40); %Usualy 50
smallholes = holes & ~bigholes;
bw = bw | smallholes;

sb2=5*(inc+1);
for i=1:sb2
    c1=xO(v)+(-(sb2/2)+i);
    for j=1:(sb2)
        r1=yO(v)+(-(sb2/2)+j);

        bw(r1,c1)=1;

    end
end
```

```
figure
imshow(bw)


[m,n]=size(bw);
% Squares=zeros(m,n);
Intersection=zeros(maxdist*4,th);
for i=1:maxdist

    for k=1:th
        b=a+(-(round(th/2))+k);

    l=length((xO(v)-b):(xO(v)+b));
    cxO1=repmat((xO(v)-b),l,1); %define x position of left line
    cxO2=repmat((xO(v)+b),l,1); %define x position of right line
    ryO1=repmat((yO(v)-b),l,1); %define y position of top line
    ryO2=repmat((yO(v)+b),l,1); %define y position of bottom line
    c=[(xO(v)-b):(xO(v)+b) cxO1' (xO(v)-b):(xO(v)+b) cxO2']; %all x
positions of square
    r=[ryO1' (yO(v)-b):(yO(v)+b) ryO2' (yO(v)-b):(yO(v)+b)]; %all y
positions of square

%         for j=1:length(c)
%              Squares(c(j),r(j))=1;
%         end

    pixels = impixel(bw,c,r); %pixel values of all pixels along the square
    S=sum(pixels);
    branchdensity(k,i)=(S(1)/(l*4));

    for g=1:length(pixels(:,1))-1
        Intersection(g,k)= abs(pixels((g+1),1) - pixels((g),1)); %Determine
if there is an intersection by seeing if pixel changes from a 0 to 1 or 1 to
0
    end

    %Eliminating noise (Branch must be 2 pixels in width)
    for g=1:length(pixels(:,1))-2
        CurrentBranchLength(g)=0;
        if Intersection(g,k)+Intersection(g+1,k)>1
            Intersection(g,k)=0;
        elseif Intersection(g,k)+Intersection(g+1,k)==1
            CurrentBranchLength(g)=sqrt((abs(xO(v)-c(g)))^2+(abs(yO(v)
```

```
−r(g)))^2);
        end
    end

    MaxBranchLength(i)=max(CurrentBranchLength)/pix2mm;



    Intersection((length(pixels(:,1))+1),k) = sum(Intersection(:,k));
    MaxInt(i,k)= max(Intersection(:,k));
    end

    branchdensity((th+1),i) = mean(branchdensity(:,i));
    NumInter(i)=mean(MaxInt(i,:))/2;
    a=a+inc;

end

branchdensity(isnan(branchdensity))=0;
BranchLengthindex = find(branchdensity((th+1),:)<0.015,1);
BranchLengthindex2 = find(branchdensity((th+1),:)<(5/l),1);

TF = isempty(BranchLengthindex);

if TF==1
    BranchLengthindex = maxdist;
end


clear branchdensity
clear BranchLengthindex
clear NumInter
clear Intersection
clear pixels
clear Density2
clear NumInter
clear MaxBranchLength
clear CurrentBranchLength
clear background
clear c r a
end

BranchLength
BranchLength2
```

```
AvgBranchNum
BranchArea

VarMatrix(1,:)=BranchLength;
VarMatrix(2,:)=AvgBranchNum;
VarMatrix(3,:)=BranchArea;
VarMatrix(4,:)=BranchLength2;
```

References

1. Swartz MA, The physiology of the lymphatic system, Adv. Drug Deliv. Rev 50, 3–20 (2001). [PubMed: 11489331]
2. Blatter C, Meijer EFJ, Nam AS, Jones D, Bouma BE, Padera TP, Vakoc BJ, In vivo label-free measurement of lymph flow velocity and volumetric flow rates using Doppler optical coherence tomography, Sci. Rep 6, 1–10 (2016). [PubMed: 28442746]
3. Dixon JB, Greiner ST, a Gashev A, Cote GL, Moore JE, Zawieja DC, Lymph flow, shear stress, and lymphocyte velocity in rat mesenteric prenodal lymphatics., Microcirculation 13, 597–610 (2006). [PubMed: 16990218]
4. Muthuchamy M, Zawieja D, Molecular regulation of lymphatic contractility., Ann. N. Y. Acad. Sci 1131, 89–99 (2008). [PubMed: 18519962]
5. Von Der Weid P, Zawieja DC, Lymphatic smooth muscle : the motor unit of lymph drainage, 36, 1147–1153 (2004).
6. Sweat RS, Sloas DC, Murfee WL, VEGF-C Induces Lymphangiogenesis and Angiogenesis in the Rat Mesentery Culture Model, Microcirculation 21, 532–540 (2014). [PubMed: 24654984]
7. Makinen T, Jussila L, Veikkola T, Karpanen T, Kettunen MI, Pulkkanen KJ, Kauppinen R, Jackson DG, Kubo H, Nishikawa S-I, Yla-Herttuala S, Alitalo K, Inhibition of lymphangiogenesis with resulting lymphedema in transgenic mice expressing soluble VEGF receptor-3, Nat Med 7, 199–205 (2001). [PubMed: 11175851]
8. Xu Y, Yuan L, Mak J, Pardanaud L, Caunt M, Kasman I, Larrivée B, Del Toro R, Suchting S, Medvinsky A, Silva J, Yang J, Thomas JL, Koch AW, Alitalo K, Eichmann A, Bagri A, Neuropilin-2 mediates VEGF-C-induced lymphatic sprouting together with VEGFR3, J. Cell Biol 188, 115–130 (2010). [PubMed: 20065093]
9. Lutter S, Xie S, Tatin F, Makinen T, Smooth muscle–endothelial cell communication activates Reelin signaling and regulates lymphatic vessel formation, J. Cell Biol 197, 837–849 (2012). [PubMed: 22665518]
10. Foubert P, Varner JA, in Methods in Molecular Biology, (2011), vol. 757, pp. 471–486.
11. Nurmi H, Saharinen P, Zarkada G, Zheng W, Robciuc MR, Alitalo K, VEGF-C is required for intestinal lymphatic vessel maintenance and lipid absorption, EMBO Mol. Med (2015).
12. Kuan EL, Ivanov S, Bridenbaugh E. a., Victora G, Wang W, Childs EW, Platt a. M., Jakubzick CV, Mason RJ, Gashev a. a., Nussenzweig M, Swartz M. a., Dustin ML, Zawieja DC, Randolph GJ, Collecting Lymphatic Vessel Permeability Facilitates Adipose Tissue Inflammation and Distribution of Antigen to Lymph Node-Homing Adipose Tissue Dendritic Cells, J. Immunol 6389, 0–3 (2015).
13. Kim H, Kataru RP, Koh GY, Inflammation-associated lymphangiogenesis: a double-edged sword?, J. Clin. Invest 124, 936–942 (2014). [PubMed: 24590279]
14. Cintolesi V, Stanton AW, BCh M, Bains SK, Cousins E, Michael Peters A, Purushotham AD, Rodney Levick J, BCh B, Mortimer PS, Constitutively Enhanced Lymphatic Pumping in the Upper Limbs of Women Who Later Develop Breast Cancer-Related Lymphedema, 14, 50–61 (2016).
15. DiSipio T, Rye S, Newman B, Hayes S, Incidence of unilateral arm lymphoedema after breast cancer: a systematic review and meta-analysis., Lancet. Oncol 14, 500–15 (2013). [PubMed: 23540561]

16. Mortimer PS, Bates DO, Brassington HD, Levick JR, Stanton AWB, Strachan DP, The prevalence of arm oedema following treatment for breast cancer, Qjm 89, 377–380 (2012).
17. Armer JM, Stewart BR, Post-breast cancer lymphedema: incidence increases from 12 to 30 to 60 months., Lymphology 43, 118–27 (2010). [PubMed: 21226414]
18. Ozturk CN, Ozturk C, Glasgow M, Platek M, Ashary Z, Kuhn J, Aronoff N, Lohman R, Djohan R, Gurunluoglu R, Free vascularized lymph node transfer for treatment of lymphedema: A systematic evidence based review, J. Plast. Reconstr. Aesthetic Surg 69, 1234–1247 (2016).
19. Schaverien MV, Badash I, Patel KM, Selber JC, Cheng MH, Vascularized Lymph Node Transfer for Lymphedema, Semin. Plast. Surg 32, 28–35 (2018). [PubMed: 29636651]
20. Raju A, Chang DW, Vascularized lymph node transfer for treatment of lymphedema: a comprehensive literature review., Ann. Surg 261, 1013–23 (2015). [PubMed: 24950271]
21. Pappalardo M, Patel K, Cheng MH, Vascularized lymph node transfer for treatment of extremity lymphedema: An overview of current controversies regarding donor sites, recipient sites and outcomes, J. Surg. Oncol 117, 1420–1431 (2018). [PubMed: 29572824]
22. Ito R, Zelken J, Yang CY, Lin CY, Cheng MH, Proposed pathway and mechanism of vascularized lymph node flaps, Gynecol. Oncol 141, 182–188 (2016). [PubMed: 26773469]
23. Yan A, Avraham T, Zampell JC, Aschen SZ, Mehrara BJ, Mechanisms of lymphatic regeneration after tissue transfer, PLoS One 6 (2011), doi:10.1371/journal.pone.0017201.
24. Tammela T, Saaristo A, Holopainen T, Lyytikkä J, Kotronen A, Pitkonen M, Abo-Ramadan U, Ylä-Herttuala S, Petrova TV, Alitalo K, Therapeutic differentiation and maturation of lymphatic vessels after lymph node dissection and transplantation, Nat. Med 13, 1458–1466 (2007). [PubMed: 18059280]
25. Bruyère F, Melen-Lamalle L, Blacher S, Roland G, Thiry M, Moons L, Frankenne F, Carmeliet P, Alitalo K, Libert C, Sleeman JP, Foidart J-M, Noël A, Modeling lymphangiogenesis in a three-dimensional culture system., Nat. Methods 5, 431–437 (2008). [PubMed: 18425139]
26. Detry B, Erpicum C, Paupert J, Blacher S, Maillard C, Bruyère F, Pendeville H, Remacle T, Lambert V, Balsat C, Ormenese S, Janssens E, Moons L, Cataldo D, Kridelka F, Carmeliet P, Thiry M, Matrix metalloproteinase-2 governs lymphatic vessel formation as an interstitial collagenase Matrix metalloproteinase-2 governs lymphatic vessel formation as an interstitial collagenase, 119, 5048–5057 (2012).
27. Browne S, Zeugolis DI, Pandit A, Collagen: Finding a Solution for the Source, Tissue Eng. Part A 19, 1491–1494 (2012).
28. Wallace DG, Rosenblatt J, Collagen gel systems for sustained delivery and tissue engineering, Adv. Drug Deliv. Rev 55, 1631–1649 (2003). [PubMed: 14623405]
29. Enemchukwu NO, Cruz-Acuña R, Bongiorno T, Johnson CT, García JR, Sulchek T, García AJ, Synthetic matrices reveal contributions of ECM biophysical and biochemical properties to epithelial morphogenesis, J. Cell Biol 212, 113–124 (2016). [PubMed: 26711502]
30. Phelps EA, Enemchukwu NO, Fiore VF, Sy JC, Murthy N, Sulchek TA, Barker TH, García AJ, Maleimide Cross-Linked Bioactive PEG Hydrogel Exhibits Improved Reaction Kinetics and Cross-Linking for Cell Encapsulation and In Situ Delivery, Adv. Mater 24, 64–70 (2012). [PubMed: 22174081]
31. Cruz-Acuña R, Quirós M, Farkas AE, Dedhia PH, Huang S, Siuda D, García-Hernández V, Miller AJ, Spence JR, Nusrat A, García AJ, Synthetic hydrogels for human intestinal organoid generation and colonic wound repair, Nat. Cell Biol 19, 1326–1335 (2017). [PubMed: 29058719]
32. Marinković A, Liu F, Tschumperlin DJ, Matrices of physiologic stiffness potently inactivate idiopathic pulmonary fibrosis fibroblasts., Am. J. Respir. Cell Mol. Biol 48, 422–30 (2013). [PubMed: 23258227]
33. Engler AJ, Sen S, Sweeney HL, Discher DE, Matrix elasticity directs stem cell lineage specification., Cell 126, 677–89 (2006). [PubMed: 16923388]
34. Keselowsky BG, Collard DM, García AJ, Integrin binding specificity regulates biomaterial surface chemistry effects on cell differentiation., Proc. Natl. Acad. Sci. U. S. A 102, 5953–5957 (2005). [PubMed: 15827122]
35. Alderfer L, Russo E, Archilla A, Coe B, Hanjaya-Putra D, Matrix stiffness primes lymphatic tube formation directed by vascular endothelial growth factor-C, FASEB J 35, 1–15 (2021).

36. Landau S, Newman A, Edri S, Michael I, Ben-Shaul S, Shandalov Y, Ben-Arye T, Kaur P, Zheng MH, Levenberg S, Investigating lymphangiogenesis in vitro and in vivo using engineered human lymphatic vessel networks, Proc. Natl. Acad. Sci. U. S. A 118, 1–12 (2021).
37. Chávez MN, Fuchs B, Moellhoff N, Hofmann D, Zhang L, Selão TT, Giunta RE, Egaña JT, Nickelsen J, Schenck TL, Use of photosynthetic transgenic cyanobacteria to promote lymphangiogenesis in scaffolds for dermal regeneration, Acta Biomater 126, 132–143 (2021). [PubMed: 33753313]
38. Knezevic L, Schaupper M, Mühleder S, Schimek K, Hasenberg T, Marx U, Priglinger E, Redl H, Holnthoner W, Engineering Blood and Lymphatic Microvascular Networks in Fibrin Matrices, Front. Bioeng. Biotechnol 5, 1–12 (2017). [PubMed: 28164082]
39. Gibot L, Galbraith T, Bourland J, Rogic A, Skobe M, Auger FA, Tissue-engineered 3D human lymphatic microvascular network for in vitro studies of lymphangiogenesis, Nat. Protoc 12, 1077–1088 (2017). [PubMed: 28448484]
40. Gibot L, Galbraith T, Kloos B, Das S, Lacroix DA, Auger FA, Skobe M, Cell-based approach for 3D reconstruction of lymphatic capillaries in vitro reveals distinct functions of HGF and VEGF-C in lymphangiogenesis, Biomaterials 78, 129–139 (2016). [PubMed: 26694987]
41. Marino D, Luginbuhl J, Scola S, Meuli M, Reichmann E, Bioengineering Dermo-Epidermal Skin Grafts with Blood and Lymphatic Capillaries, Sci. Transl. Med 6, 221ra14–221ra14 (2014).
42. Campbell KT, Curtis MB, Massey JM, Wysoczynski K, Hadley DJ, George SC, Silva EA, Isolating and characterizing lymphatic endothelial progenitor cells for potential therapeutic lymphangiogenic applications, Acta Biomater (2021), doi:10.1016/j.actbio.2021.08.005.
43. Kassis T, Skelton HM, Lu IM, Moorhead AR, Dixon JB, An Integrated In Vitro Imaging Platform for Characterizing Filarial Parasite Behavior within a Multicellular Microenvironment, PLoS Negl. Trop. Dis 8 (2014), doi:10.1371/journal.pntd.0003305.
44. Mas-Moruno C, Cavalcanti-Adam EA, Reuning U, Geiger B, Neubauer S, Kessler H, Maltsev OV, Notni J, Kapp TG, Zarka R, Wester H-J, Spatz J, Rechenmacher F, A Comprehensive Evaluation of the Activity and Selectivity Profile of Ligands for RGD-binding Integrins, Sci. Rep 7, 1–13 (2017). [PubMed: 28127051]
45. Bax DV, Bernard SE, Lomas A, Morgan A, Humphries J, Shuttleworth CA, Humphries MJ, Kielty CM, Cell Adhesion to Fibrillin-1 Molecules and Microfibrils Is Mediated by α5β1 and αvβ3 Integrins, J. Biol. Chem 278, 34605–34616 (2003). [PubMed: 12807887]
46. Garanger E, Boturyn D, Coll JL, Favrot MC, Dumy P, Multivalent RGD synthetic peptides as potent αvβ 3 integrin ligands, Org. Biomol. Chem 4, 1958–1965 (2006). [PubMed: 16688341]
47. Kosinski AM, Sivasankar MP, Panitch A, Varying RGD concentration and cell phenotype alters the expression of extracellular matrix genes in vocal fold fibroblasts, J. Biomed. Mater. Res. Part A 103, 3094–3100 (2015).
48. Yang F, Williams CG, Wang DA, Lee H, Manson PN, Elisseeff J, The effect of incorporating RGD adhesive peptide in polyethylene glycol diacrylate hydrogel on osteogenesis of bone marrow stromal cells, Biomaterials 26, 5991–5998 (2005). [PubMed: 15878198]
49. Cao X, Yu WQ, Qiu J, Zhao YF, Zhang YL, Zhang FQ, RGD peptide immobilized on TiO 2 nanotubes for increased bone marrow stromal cells adhesion and osteogenic gene expression, J. Mater. Sci. Mater. Med 23, 527–536 (2012). [PubMed: 22143905]
50. Zhao N, Battig MR, Xu M, Wang X, Xiong N, Wang Y, Development of a Dual-Functional Hydrogel Using RGD and Anti-VEGF Aptamer, Macromol. Biosci 17, 1700201 (2017).
51. Cruz-Acuña R, Mulero-Russe A, Clark AY, Zent R, García AJ, Identification of matrix physicochemical properties required for renal epithelial cell tubulogenesis by using synthetic hydrogels, J. Cell Sci 132 (2019), doi:10.1242/jcs.226639.
52. Lutolf MP, Lauer-Fields JL, Schmoekel HG, Metters AT, Weber FE, Fields GB, Hubbell JA, Synthetic matrix metalloproteinase-sensitive hydrogels for the conduction of tissue regeneration: Engineering cell-invasion characteristics, Proc. Natl. Acad. Sci 100, 5413–5418 (2003). [PubMed: 12686696]
53. Helm C-LE, Fleury ME, Zisch AH, Boschetti F, Swartz MA, Synergy between interstitial flow and VEGF directs capillary morphogenesis in vitro through a gradient amplification mechanism, Proc. Natl. Acad. Sci 102, 15779–15784 (2005). [PubMed: 16249343]

54. Okazaki T, Ni A, Ayeni OA, Baluk P, Yao L-C, Vossmeyer D, Zischinsky G, Zahn G, Knolle J, Christner C, McDonald DM, α5β1 Integrin Blockade Inhibits Lymphangiogenesis in Airway Inflammation, Am. J. Pathol 174, 2378–2387 (2009). [PubMed: 19443705]
55. Brooks PC, Clark RA, Cheresh DA, Requirement of vascular integrin alpha v beta 3 for angiogenesis, Science (80-.). 264, 569 LP – 571 (1994).
56. Gashev AA, Davis MJ, Zawieja DC, Inhibition of the active lymph pump by flow in rat mesenteric lymphatics and thoracic duct, J. Physiol 540, 1023–1037 (2002). [PubMed: 11986387]
57. Davis MJ, Scallan JP, Wolpers JH, Muthuchamy M, a Gashev A, Zawieja DC, Intrinsic increase in lymphangion muscle contractility in response to elevated afterload., Am. J. Physiol. Heart Circ. Physiol 303, H795–808 (2012). [PubMed: 22886407]
58. a Gashev A, Davis MJ, Delp MD, Zawieja DC, Regional variations of contractile activity in isolated rat lymphatics., Microcirculation 11, 477–92 (2004). [PubMed: 15371129]
59. McHale NG, Roddie IC, Pumping activity in isolated segments of bovine mesenteric lymphatics, J. Physiol 261, 70–72 (1975).
60. Jamalian S, Davis MJ, Zawieja DC, Moore JE, Network Scale Modeling of Lymph Transport and Its Effective Pumping Parameters, PLoS One 11, 1–18 (2016).
61. Güç E, Briquez PS, Foretay D, Fankhauser MA, Hubbell JA, Kilarski WW, Swartz MA, Local induction of lymphangiogenesis with engineered fibrin-binding VEGF-C promotes wound healing by increasing immune cell trafficking and matrix remodeling, Biomaterials 131, 160–175 (2017). [PubMed: 28410495]
62. Helm CLE, Zisch A, Swartz MA, Engineered blood and lymphatic capillaries in 3-D VEGF-fibrin-collagen matrices with interstitial flow, Biotechnol. Bioeng 96, 167–176 (2007). [PubMed: 17133613]
63. Maltzman JS, Reed HO, Kahn ML, HA-ving lymphatics improves lung transplantation, J. Clin. Invest 125, 3999–4001 (2015). [PubMed: 26524589]
64. Wu M, Du Y, Liu Y, He Y, Yang C, Wang W, Gao F, Low molecular weight hyaluronan induces lymphangiogenesis through LYVE-1-mediated signaling pathways, PLoS One 9 (2014), doi:10.1371/journal.pone.0092857.
65. Worley DR, Hansen RJ, Wittenburg LA, Chubb LS, Gustafson DL, Docetaxel Accumulates in Lymphatic Circulation Following Subcutaneous Delivery Compared, 5078, 5071–5078 (2016).
66. Swaroop MN, Ferguson CM, Horick NK, Skolny MN, Miller CL, Jammallo LS, Brunelle CL, O'Toole JA, Isakoff SJ, Specht MC, Taghian AG, Impact of adjuvant taxane-based chemotherapy on development of breast cancer-related lymphedema: results from a large prospective cohort, Breast Cancer Res. Treat 151, 393–403 (2015). [PubMed: 25940996]
67. Harris AR, Perez MJ, Munson JM, Docetaxel facilitates lymphatic-tumor crosstalk to promote lymphangiogenesis and cancer progression, , 1–16 (2018).
68. Phelps EA, Landázuri N, Thulé PM, Taylor WR, García AJ, Bioartificial matrices for therapeutic vascularization, Proc. Natl. Acad. Sci 107, 3323–3328 (2010). [PubMed: 20080569]
69. Shekaran A, García JR, Clark AY, Kavanaugh TE, Angela S, Guldberg RE, García AJ, Bone Regeneration using an Alpha 2 Beta 1 Integrin-Specific Hydrogel as a BMP-2 Delivery Vehicle, 35, 5453–5461 (2015).
70. Becker C, Assouad J, Riquet M, Hidden G, Postmastectomy Lymphedema, Ann. Surg 243, 313–315 (2006). [PubMed: 16495693]
71. Hartiala P, Suominen S, Suominen E, Kaartinen I, Kiiski J, Viitanen T, Alitalo K, Saarikko AM, Phase 1 Lymfactin® Study: Short-term Safety of Combined Adenoviral VEGF-C and Lymph Node Transfer Treatment for Upper Extremity Lymphedema, J. Plast. Reconstr. Aesthetic Surg 73, 1612–1621 (2020).
72. Hadamitzky C, Zaitseva TS, Bazalova-Carter M, Paukshto MV, Hou L, Strassberg Z, Ferguson J, Matsuura Y, Dash R, Yang PC, Kretchetov S, Vogt PM, Rockson SG, Cooke JP, Huang NF, Aligned nanofibrillar collagen scaffolds – Guiding lymphangiogenesis for treatment of acquired lymphedema, Biomaterials 102, 259–267 (2016). [PubMed: 27348849]
73. Pabst R, Breves G, Buettner M, Schindewolffs L, Hadamitzky C, VEGF-C improves regeneration and lymphatic reconnection of transplanted autologous lymph node fragments: An animal model for secondary lymphedema treatment, Immunity, Inflamm. Dis 2, 152–161 (2014).

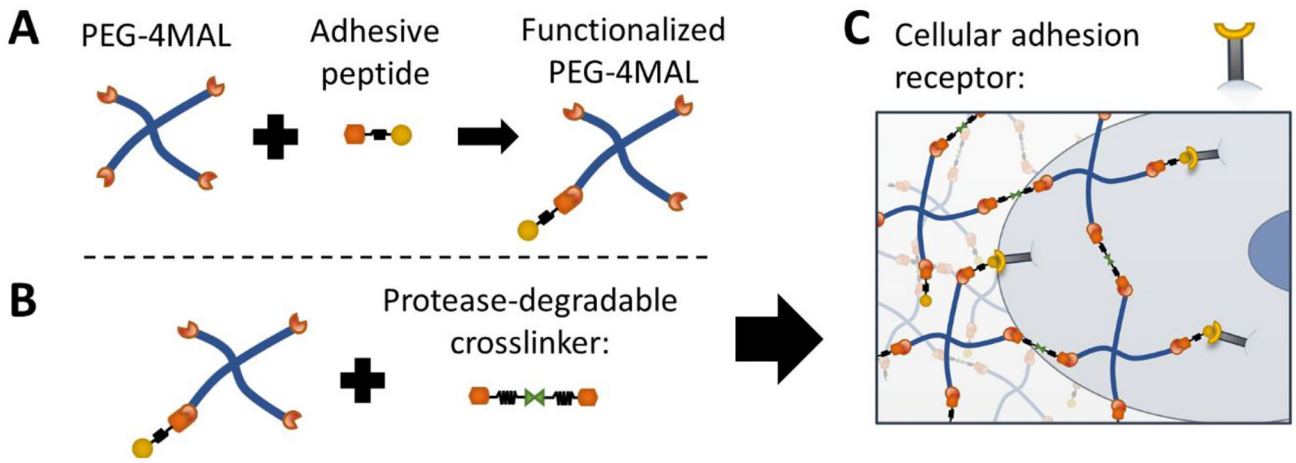

Figure 1:
Schematic of 4 arm PEG hydrogel functionalized with adhesive peptides and protease-degradable crosslinker. (A) PEG-4MAL is functionalized with adhesive peptides bound to thiol groups. (B). PEG-4MAL functionalized with adhesive peptides reacts with protease degradable crosslinks forming (C) the fully functionalize hydrogel allowing for cellular adhesion and degradation.

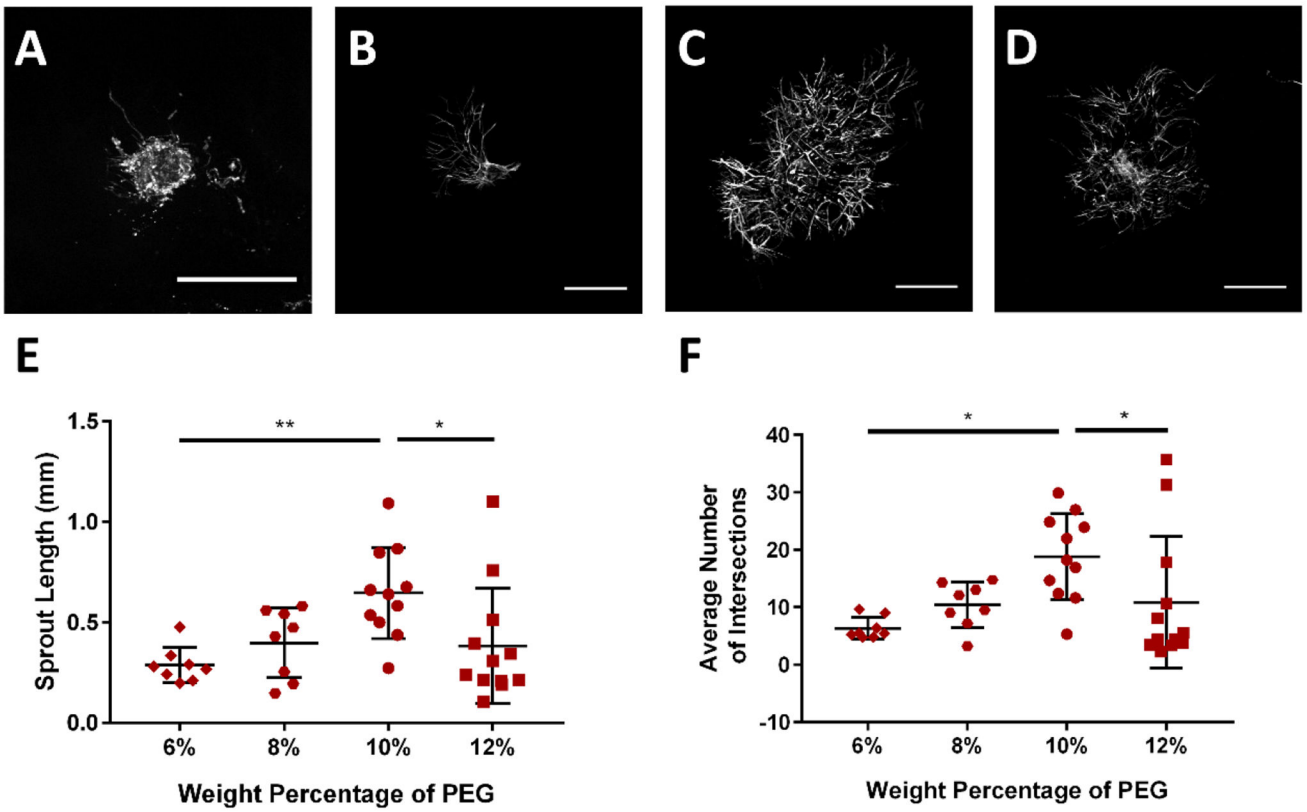

Figure 2:

PEG hydrogel polymer weight percentage (WP) controls lymphatic sprouting. Representative images of collecting vessel segments at day 7 cultured in (A) 6% PEG, (B) 8% PEG, (C) 10% PEG, and (D) 12% PEG gels presenting 2.0 mM RGD. Images are of vessels labeled with Calcein-AM indicating live cells. Scale bar = 500 μm. (E) Sprout length and (F) average number of intersections exhibit maximal values at intermediate gel polymer densities. Each point represents a biologically independent sample (sample size: 6% PEG = 8, 8% PEG = 8, 10% PEG = 11, 12% PEG = 12). Data analyzed using Kruskal-Wallis test followed by Dunn's multiple comparisons.

* $p<0.05$, ** $p<0.01$.

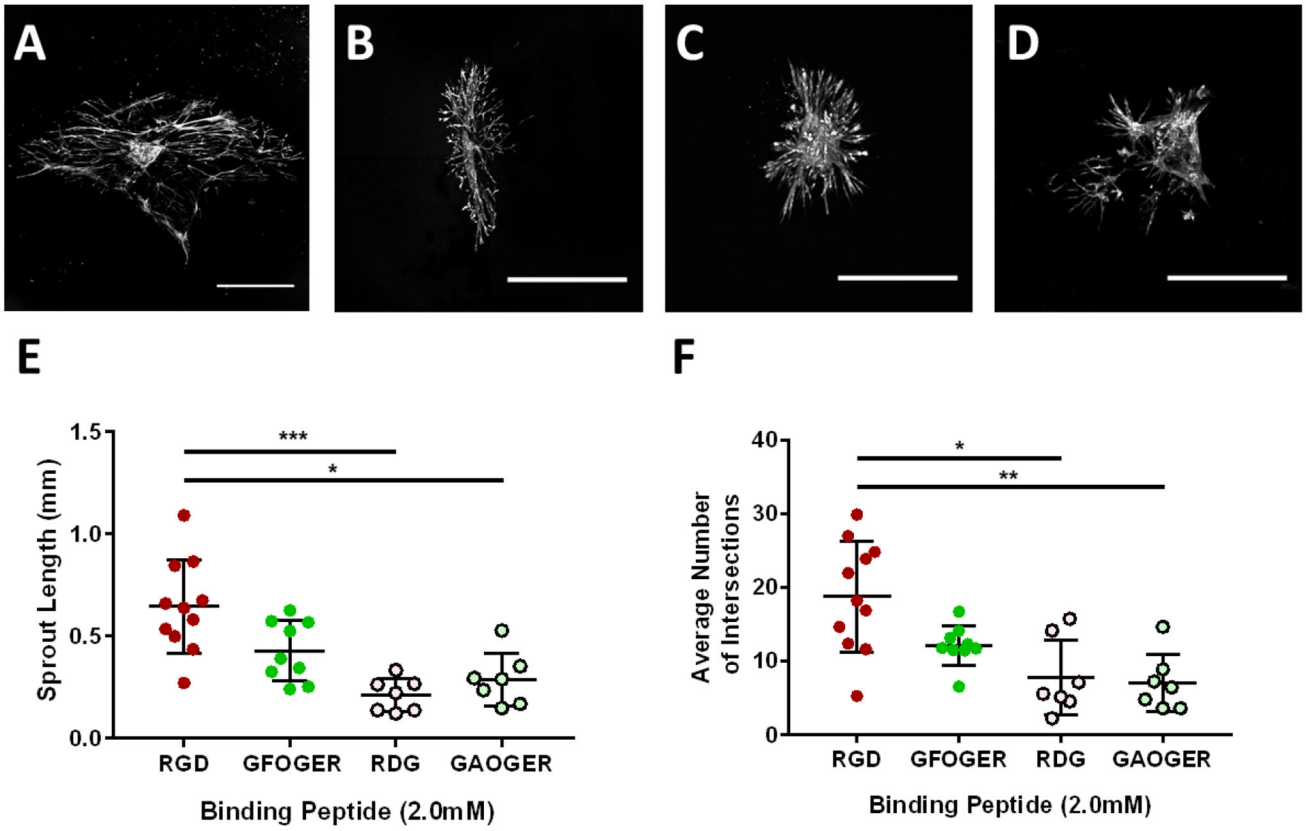

Figure 3:

RGD adhesive peptide promotes lymphatic sprout length and number in fully degradable PEG hydrogels. Representative images of collecting vessel segments stained with Calcein-AM at day 7 cultured in 10% PEG gels presenting (A) RGD, (B) GFOGER, (C) RDG, and (D) GAOGER peptides (2.0 mM). Scale bar = 500 μm. Quantification of (E) sprout length and (F) average number of intersections at day 7 compared to the GFOGER adhesive peptide and the scrambled control peptides RDG and GAOGER. Each point represents a biologically independent sample (sample size: RGD = 11, GFOGER = 9, RDG = 7, GAOGER = 7). Data analyzed using Kruskal-Wallis test followed by Dunn's multiple comparisons. * $p<0.05$, ** $p<0.01$, *** $p<0.001$.

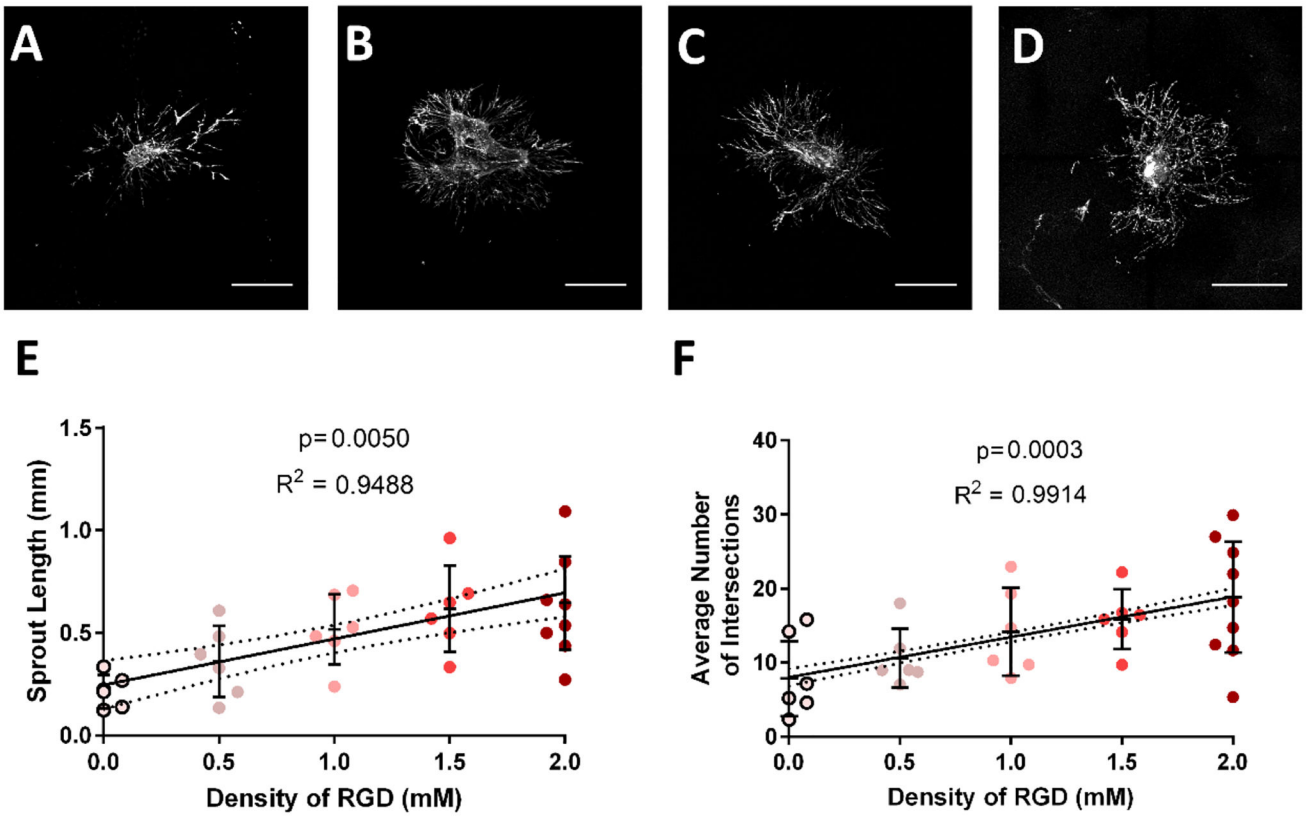

Figure 4:

Sprouting intersections and length increases with increasing concentration of RGD in fully degradable, 10% PEG hydrogels. Representative images of collecting vessel segments labeled with Calcein-AM at day 7 cultured in (A) 0.5 mM RGD, (B) 1.0 mM RGD, (C) 1.5 mM RGD and (D) 2.0 mM RGD conditions. Scale bar = 500 μm. There was no significant change in (E) sprout length or (F) average number of intersections at tested concentrations above 0.0 mM RGD. Each point represents a biologically independent sample (sample size: 0.0 mM RGD = 6, 0.5 mM RGD = 6, 1.0 mM RGD = 6, 1.5 mM RGD = 6, 2.0 mM RGD = 11). Linear regression shows the dependency of sprout length and average number of intersections on RGD density. Dotted lines above and below the regression represent 95% confidence intervals and the p-values reflect the results of an F-test to determine the significance of a non-zero slope. * $p<0.05$, ** $p<0.01$

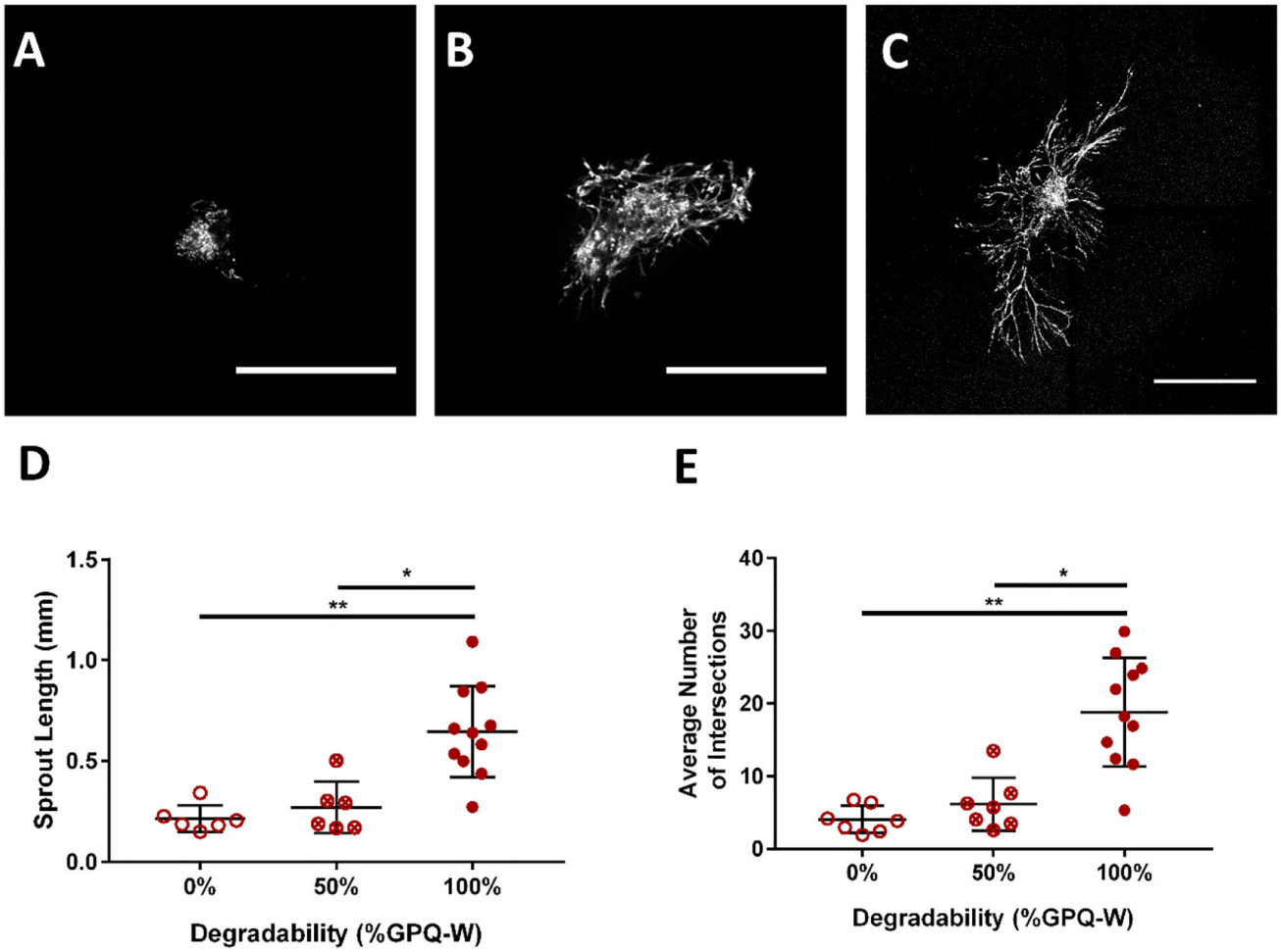

Figure 5:

Hydrogel protease-degradability is required for lymphatic sprouting in PEG hydrogels. Rat LLVs were encapsulated in 10% PEG gels presenting 2.0 mM RGD and crosslinked with the crosslinker indicated. Representative images of collecting vessel segments labeled with Calcein-AM at day 7 cultured in (A) 0% degradable, (B) 50% degradable, and (C) 100% degradable conditions. Scale bar = 500 μm. (D) Lymphatic collecting vessels cultured with 0% of 50% degradability had significantly reduced sprout length by day 7 compared to the fully (100%) degradable condition. (E) Lymphatic collecting vessels cultured with 0% of 50% degradability had significantly reduced average number of sprouts coming from the implanted vessel segment by day 7 compared to the fully (100%) degradable condition. Each point represents a biologically independent sample (sample size: 0% GPQ-W = 7, 50% GPQ-W = 6, 100% GPQ-W = 11). Data analyzed by Kruskal-Wallis test followed by Dunn's multiple comparisons. * $p<0.05$, ** $p<0.01$.

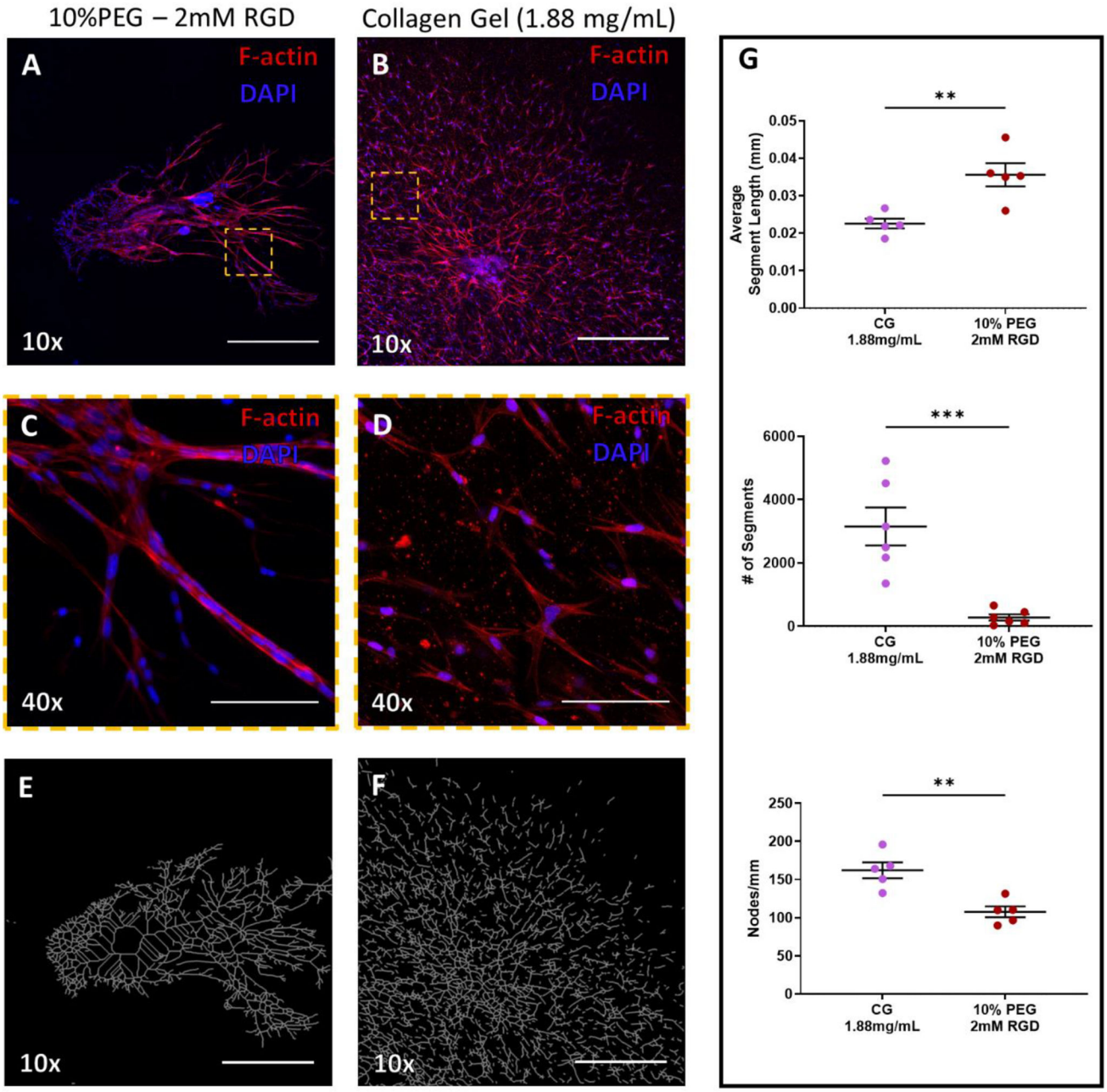

Figure 6:

Culture of Lymphatic vessel segments in tunable PEG-4MAL hydrogels (A & B) F-actin (red) staining of lymphatic tissue at day 7 of culture in PEG hydrogel (fully degradable, 10% PEG − 2.0 mM RGD) or collagen gel (1.88 mg/mL), respectively. DAPI stain of nuclei in blue. Scale bars = 500 μm. (C & D) Indicated regions in panels (A) and (B), respectively, imaged with higher objective magnification demonstrates the varied organization of cells at 7 days of culture. Scale bar = 100 μm. (E & F) Simplified branching network produced by angiogenesis analyzer software based on F-actin staining in the PEG hydrogel (A) and collagen gel (B), respectively. (G) Sprouting metrics of average segment length, number of segments, and nodes/mm of PEG gel and collagen gel replicates.

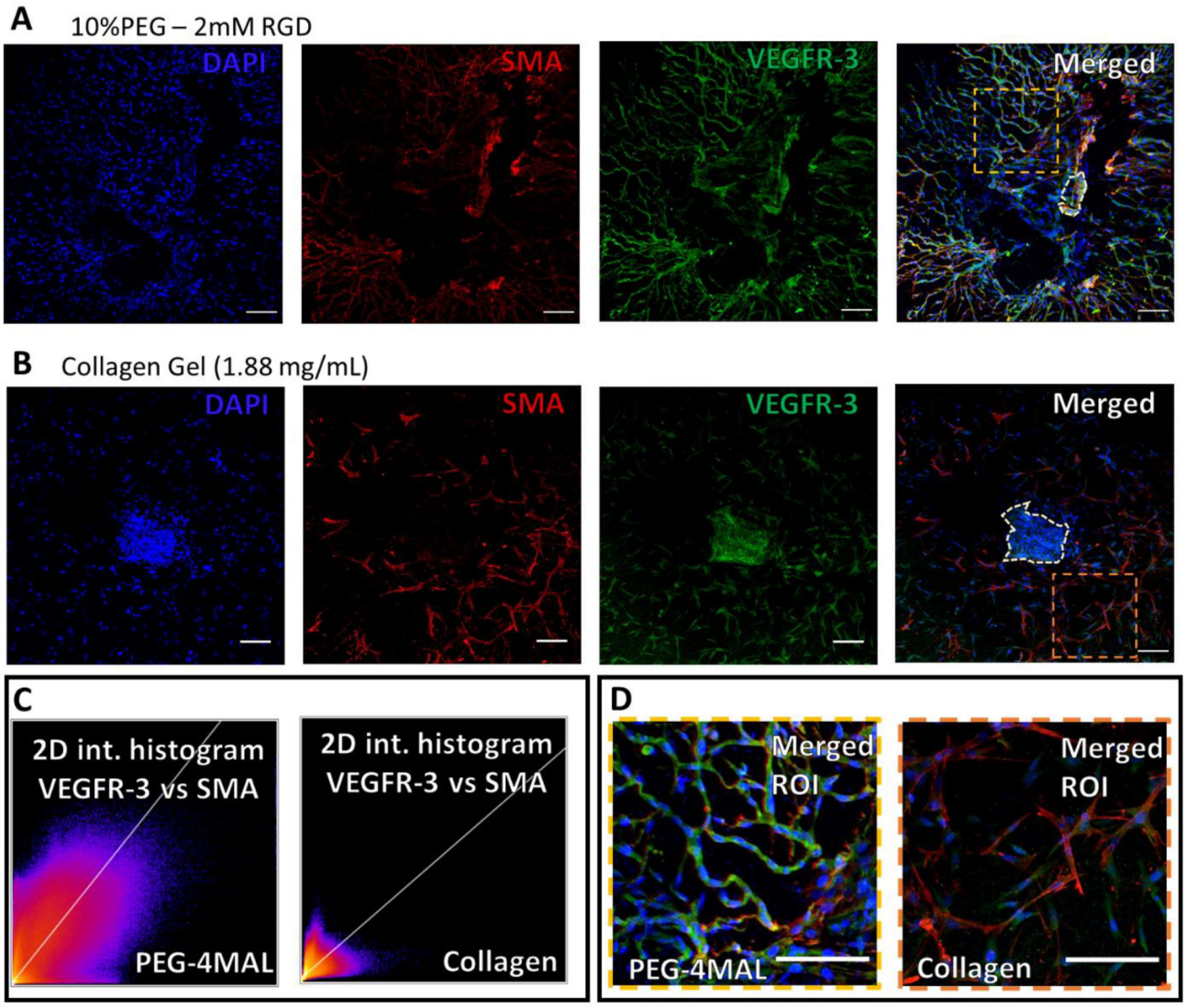

Figure 7: LEC and LMC distribution in lymphatic sprouting network after 7-day culture in hydrogels.

(**A**) Staining of vessel segments cultured in fully degradable, 10%PEG − 2 mM RGD hydrogels for nuclei (blue), α-smooth muscle actin (red), endothelial nitric oxide synthase (gray), and vascular endothelial growth factor receptor-3 (green), respectively. 2D intensity histograms demonstrating the correlation of VEGFR3 and SMA in the PEG-4MAL gel and collagen gel (B) Similar staining for vessel segments cultured in collagen gels (1.88 mg/mL). (**I**) Zoomed in and merged image of the vessel segment sprouting phenotype in PEG hydrogel. From region indicated in panel (**A**). (**J**) Zoomed in, merged, image of vessel segment sprouting phenotype in collagen gel (1.88 mg/mL). From region indicated in panel (**E**). Scale bars=100 μm.